Article

Speckle Reduction by Directional Coherent Anisotropic Diffusion

Guo Zhang [1,2], **Fengcheng Guo [1,*]**, **Qingjun Zhang [2,3]**, **Kai Xu [1]**, **Peng Jia [4]** and **Xiaoyun Hao [5]**

[1] State Key Laboratory of Information Engineering in Surveying Mapping and Remote Sensing, Wuhan University, Wuhan 430079, China; guozhang@whu.edu.cn (G.Z.); kaixu@whu.edu.cn (K.X.)
[2] Collaborative Innovation Center of Geospatial Technology, Wuhan University, Wuhan 430079, China; zhangqj@cast.casc
[3] China Academy of Space Technology, Beijing 100094, China
[4] China Satellite Navigation Office, Beijing 100034, China; jiap@beidou.gov.cn
[5] Shandong Aerospace Electro-Technology Institute, Yantai 264000, China; hxy_2018@163.com
* Correspondence: fchguo@whu.edu.cn; Tel.: +86-186-0275-1869

check for updates

Abstract: To effectively balance speckle smoothing and preservation of edges and radiation, a novel anisotropic diffusion filter was developed that uses a directional coherent coefficient. The proposed filter effectively improves the edge detection operator of a traditional anisotropic diffusion filter. The new edge detection operator calculates 16 direction coherence coefficients to avoid the interference of the edge direction. For the diffusion function, the proposed method directly uses the detected directional coherent edge as the diffusion coefficient, which simplifies the calculation of the diffusion function and avoids the adverse effects of inaccurate estimation of the diffusion function threshold for a traditional anisotropic diffusion filter. The influence of the number of iterations and time steps on the proposed filter was analyzed. A series of experiments was conducted with a simulated image and three real synthetic-aperture radar images from different sensors. The results confirmed that the proposed method not only significantly reduces speckle but also effectively preserves the edge and radiation information of images.

Keywords: synthetic aperture radar; speckle reduction; anisotropic diffusion; directional coherent edge detection

1. Introduction

A synthetic aperture radar (SAR) system transmits a signal and receives the echo signal from a scene to generate an image, as shown in Figure 1a. A resolution cell of the echo signal usually contains several scatterers. When no one scatterer yields a reflected signal much stronger than the others (i.e., a distributed target), the received echo signal can be viewed as the incoherent sum of several backscattered waves [1]. Speckle is inevitably generated by the above SAR coherent imaging system, which carries real electromagnetic information of the observed surface [1,2]. However, this information is considered to be noise for image analysis because speckle hides many details of the observed scene. As shown in Figure 1b, much of the real information of objects is obscured by abundant speckle compared with the real optical image shown in Figure 1c. Thus, speckle noise need to be effectively suppressed before SAR image analysis.

Speckle suppression has been studied for decades, and many excellent methods have been developed. These denoising filters are related to different fields, such as digital speckle pattern interferometry fringes despeckling [3–5], ultrasound image despeckling [6–8], and SAR image

despeckling [9–23]. The area of speckle denoising is very broad [3], so only some methods directly related to this paper are reviewed here. Usually, the often used despeckling filters can be classified into three categories: spatial domain (SD) filtering, transform domain (TD) filtering, and anisotropic diffusion (AD) filtering. The most widely cited and applied SD filters include the Lee [9–12], Frost [13,14], and Kuan [15,16] filters. SD filters can greatly reduce speckle, although the performance relies heavily on the choice of the local window size and orientation [17]. TD filters often use the wavelet transform [18], curvelet transform [19], and shearlet transform [20] for speckle suppression. However, although TD filters suppress noise well, they have high computational complexity [21]. For speckle suppression, a good speckle filter should provide excellent speckle smoothing, edge preservation, and radiometric preservation [1,17,21]. AD filters use a diffusion coefficient to effectively balance these three aspects [22,23].

(a)　　　　　　　　　　　　　　　　(b)　　　　　　　　　　　　　　　　(c)
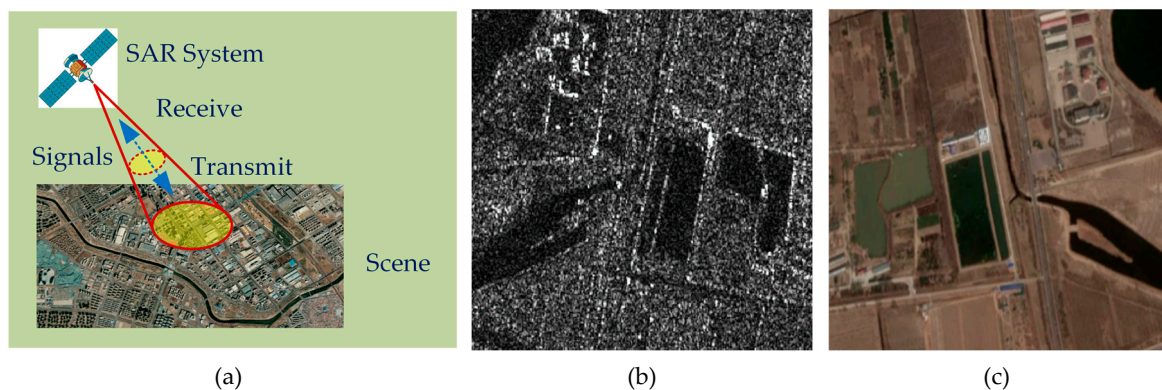
Figure 1. (**a**) Synthetic aperture radar (SAR) imaging system, (**b**) actual SAR image, and (**c**) corresponding optical image.

In 1990, Peron and Malik designed the earliest AD filter for suppressing additive noise [24]. They proposed a nonlinear partial differential equation (PDE) for the Peron–Malik (P–M) method. Solving the PDE is an effective strategy for suppressing noise with AD filters. However, the speckle in SAR images is widely considered to be multiplicative noise. Yu and Acton proposed the speckle reducing anisotropic diffusion (SRAD) filter [25] to adapt the P–M method to multiplicative noise. The SRAD filter applies a novel diffusion coefficient that exploits the instantaneous coefficient of variation to update the PDE of the P–M method to realize edge-sensitive anisotropy detection in SAR images. Subsequent improved AD filters [26–29] have mostly been based on the updated SRAD PDE. These improvements mostly focused on enhancing edge preservation, radiometric preservation, and speckle smoothing. The key has been to obtain an effective edge detection function. The detail preserving anisotropic diffusion (DPAD) [26] filter improves the estimation of the coefficient of variation for both the signal and noise. The adaptive window anisotropic diffusion (AWAD) [27] filter uses the adaptive window method to calculate the instantaneous coefficient of variation. The weighted Euclidean distance anisotropic diffusion (WEDAD) [21] filter improves the edge detection operator by using weighted Euclidean distances. Other improved AD filters have mainly focused on enhancing edge detection. These above improvements all enhance the filtering effect. However, the good denoising effects of these AD filters rely on accurate estimation of parameters such as the threshold of the diffusion function or the mean and variance of noise.

This paper proposes the directional coherent anisotropic diffusion (DCAD) filter, which uses the directional coherent coefficient for effective edge detection in all directions and does not require estimating the mean and variance of noise. The directional coherent coefficient directly acts as the diffusion coefficient to avoid the adverse effects of inaccurate estimation of the diffusion function threshold. The rest of this paper presents the development and experimental verification of the proposed method.

2. Materials and Methods

2.1. Speckle Model

The imaging output image of an echo signal is usually a single look complex (SLC), which consists of real and imaginary components. The SLC data carry both intensity and phase information. However, most current despeckling methods use intensity or amplitude images. An intensity image can be generated by the sum of the squares of these two components of the SLC image:

$$I = Re \cdot Re + Im \cdot Im \tag{1}$$

where I is the intensity and Re and Im are the real and imaginary components, respectively, of the SLC data. The amplitude can be further generated from the root of the intensity. Frery et al. [30] modeled the probability density function (PDF) of speckle. The PDF of the speckle S can be characterized in intensity and amplitude images, respectively, as follows:

$$f_{intensity}(S) = \frac{L^L}{\Gamma(L)} S^{L-1} \exp(-LS) \tag{2}$$

$$f_{amplitude}(S) = \frac{2L^L}{\Gamma(L)} S^{2L-1} \exp(-LS^2) \tag{3}$$

where L is the number of looks and $\Gamma(x)$ is the gamma function.

The PDF describes the statistical characteristics of the speckle. The widely recognized multiplicative noise model can further illustrate the effect of speckle on the true signal and is given as follows:

$$I_O(x, y) = I_{NF}(x, y) \cdot S(x, y) \tag{4}$$

where I_O is the observed intensity and amplitude images, I_{NF} is the noise-free intensity and amplitude images, S is the speckle, and (x, y) is the pixel position.

2.2. Anisotropic Diffusion Filtering

The P–M method [24] is an AD filter and proposes the following nonlinear PDE for smoothing images:

$$\begin{cases} \frac{\partial I}{\partial t} = div[c(|\nabla I|) \cdot \nabla I] \\ I(t = 0) = I_0 \end{cases} \tag{5}$$

Here, div, ∇, and $\|$ denote the divergence, gradient operators, and magnitude, respectively. I_0 is the initial SAR image, and $c(x)$ is the diffusion coefficient, which has the following two forms:

$$c(x) = \frac{1}{1 + (x/k)^2} \tag{6}$$

$$c(x) = \exp\left[-(x/k)^2\right] \tag{7}$$

where k is used for edge detection.

In the P–M method, the diffusion coefficient is designed for AD filters. The value of $c(x)$ is 0 to 1, which is calculated with the edge detection operator k according to Equation (6) or (7). If $|\nabla I| \gg k$, then $c(|\nabla I|)$ trends to 0, and an all-pass filter is used. If $|\nabla I| \ll k$, then $c(|\nabla I|)$ trends to 1, and an isotropic diffusion filter is used [24]. The above analysis shows that the design of the diffusion coefficient plays an important role in AD filters. However, the original diffusion coefficient is designed for additive noise. For multiplicative noise, the SRAD filter provides two new diffusion coefficients:

$$c(q) = \frac{1}{1 + \left[q^2 - q_0^2\right] / \left[q_0^2\left(1 + q_0^2\right)\right]} \tag{8}$$

$$c(q) = \exp\left\{-\left[q^2 - q_0^2\right] / \left[q_0^2\left(1 + q_0^2\right)\right]\right\} \tag{9}$$

where q_0 is the speckle scale function and q is the instantaneous coefficient of variation. This can be modeled as follows:

$$q = \sqrt{\frac{(1/2)(|\nabla I|/I)^2 - (1/4^2)\left(\left|\nabla^2 I\right|/I\right)^2}{\left[1 + (1/4)\left(\left|\nabla^2 I\right|/I\right)\right]^2}} \tag{10}$$

Based on the new diffusion coefficient, the PDE in Equation (5) can be updated as follows:

$$\begin{cases} \frac{\partial I}{\partial t} = div[c(q) \cdot \nabla I] \\ I(t = 0) = I_0 \end{cases} \tag{11}$$

The SRAD filter uses an iterative Jacobi method to numerically solve the PDE given in Equation (11). Specific solution steps are given by Yu and Acton [25]. The PDE of the SRAD filter can be numerically approximated as

$$I_{i,j}^{n+1} = I_{i,j}^n + \frac{\Delta t}{4} d_{i,j}^n, \tag{12}$$

where

$$d_{i,j}^n = \frac{1}{h^2}\left[c_{i+1,j}^n\left(I_{i+1,j}^n - I_{i,j}^n\right) + c_{i,j}^n\left(I_{i-1,j}^n - I_{i,j}^n\right) + c_{i,j+1}^n\left(I_{i,j+1}^n - I_{i,j}^n\right) + c_{i,j}^n\left(I_{i,j-1}^n - I_{i,j}^n\right)\right] \tag{13}$$

Here, n is the number of iterations and Δt and h denote a sufficiently small time and spatial step size, respectively.

2.3. Directional Coherent Edge Detection

As noted previously, the core of applying an AD filter to a SAR image with abundant speckle is the construction of an edge detection operator. Speckle is a kind of random noise, and edge information usually has structural characteristics. Using structural information is an effective strategy for obtaining edge information. The edges usually show sharp changes in pixels, as shown in Figure 2. Figure 2a shows an obvious edge feature. Figure 2b shows a three-dimensional image with a significant pixel difference at the edge. Therefore, this pixel difference feature can be used to detect edge information.
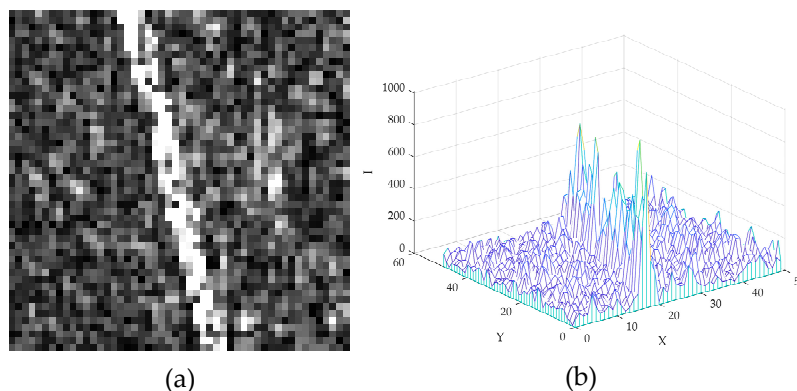

(a)   (b)

Figure 2. (**a**) local SAR image of GF-3 and (**b**) its three-dimensional display.

The coherence coefficient [31,32] is introduced here to exploit this characteristic of edge information:

$$r = \frac{\sum\limits_{n=1}^{N} c_{1n} \cdot c_{2n}^*}{\sqrt{\sum\limits_{n=1}^{N} |c_{1n}|^2 \cdot \sum\limits_{n=1}^{N} |c_{2n}|^2 \cdot}} \tag{14}$$

where r is the coherence coefficient, N is the n neighborhood pixels around the center pixel, * is the complex conjugate, and c_1 and c_2 are the SLC SAR images of the same scene.

When the two calculated regions are identical, the coherence coefficient is 1. When there is pixel difference between the two compared regions, the coherence coefficient is far from 1 and can reach 0 in extreme cases. In other words, a greater difference between the two regions results in a smaller coherence coefficient. The edge region is determined by a large pixel difference. Therefore, the coherence coefficient can indicate the possibility of a detected edge.

To use the coherence coefficient to detect edge information, some changes need to be implemented. The coherence between two images needs to be transformed to calculate the coherence between two regions of an image. In addition, the intensity or amplitude is usually used for filtering, so the coherence coefficient also needs to be changed to be applicable to intensity or amplitude data. The improved coherent coefficient model can be written as follows:

$$r = \frac{\sum I_A \cdot I_B}{\sqrt{\sum I_A^2 \cdot \sum I_B^2}} \tag{15}$$

where A and B represent two symmetrical regions for calculating the coherence coefficient and r is the coherence coefficient with a range from 0 to 1. In theory, when R approaches 1, the two compared regions are close and can be regarded as homogeneous, while the opposite holds true for marginal regions. The detailed calculation process for edge detection based on the coherence coefficient is shown in Figure 3a.
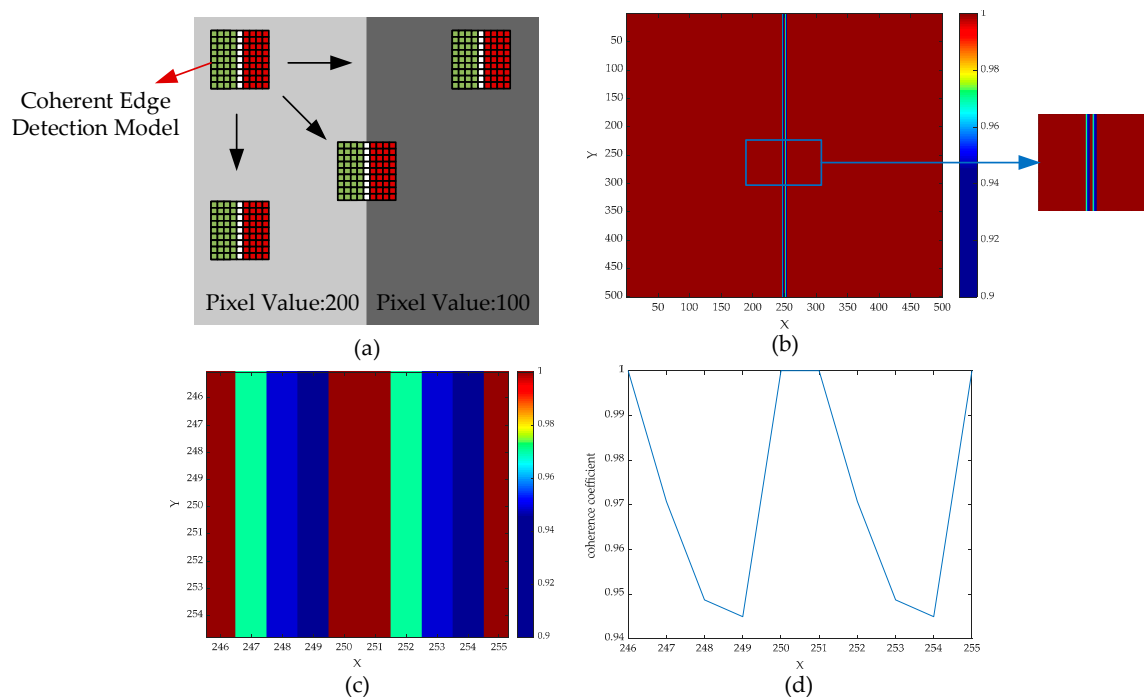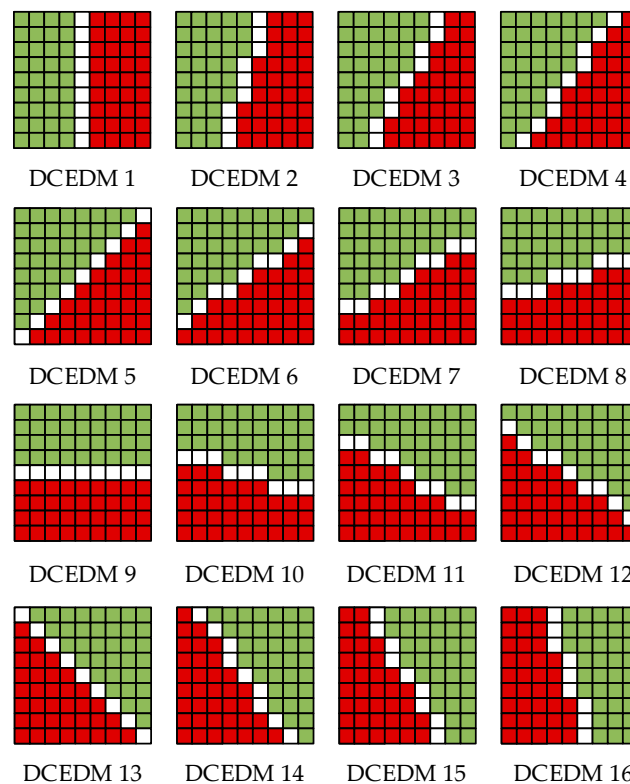

Figure 3. Results of the coherent edge detection calculation: (**a**) flowchart of the calculation; (**b**) coherent coefficient of the test image; (**c**) local display of (**b**); (**d**) line graph of any line edge region of (**c**).

To clarify the process of coherence coefficient edge detection, a specific operation was performed on a test image. The test image in Figure 3a was generated by MATLAB R2019b and consists of two groups of pixel values: 200 and 100. Areas in the test image with the same pixels were considered to be homogeneous, and the boundary area with different pixels was considered to be the edge. The 9×9 rectangular window composed of green, white, and red is the coherent edge detection model. The coherence edge detection model was moved from left to right and from top to bottom, and Equation (15) was used to calculate the coherence coefficient of each pixel in sequence. The green and red regions were represented by *A* and *B*, respectively, in Equation (15) while white regions were not included in the calculation. Figure 3b,d show the results of the above calculation. Figure 3b visualizes the obtained coherent edge detection coefficient. The yellow region shows the effectively detected edge region and corresponds to the edge region of Figure 3a, which preliminarily indicates the validity of the edge detection. However, when the edge region of the red rectangular window in Figure 3b was enlarged, an area with the same color as the homogeneous area in the middle of the edge region was observed. To further observe the edge region, it was further enlarged, as shown in Figure 3c, and an arbitrary line was intercepted to draw the line graph shown in Figure 3d for the coherent edge detection coefficient. The data for the edge center region and homogeneous region generated the same coherent edge detection coefficient, which is obviously unfavorable. This was caused by the identical pixel values in regions *A* and *B*. To solve this problem, the directional coherent edge detection model (DCEDM) is proposed and is shown in Figure 4. The DCEDM is also necessary for detecting edge information in different directions. The DCEDM consists of 16 different models. To calculate the directional coherence edge detection coefficients, the coherence edge detection coefficients in 16 directions are calculated one by one. The minimum value is the final directional coherent edge detection value and can be modeled as follows:
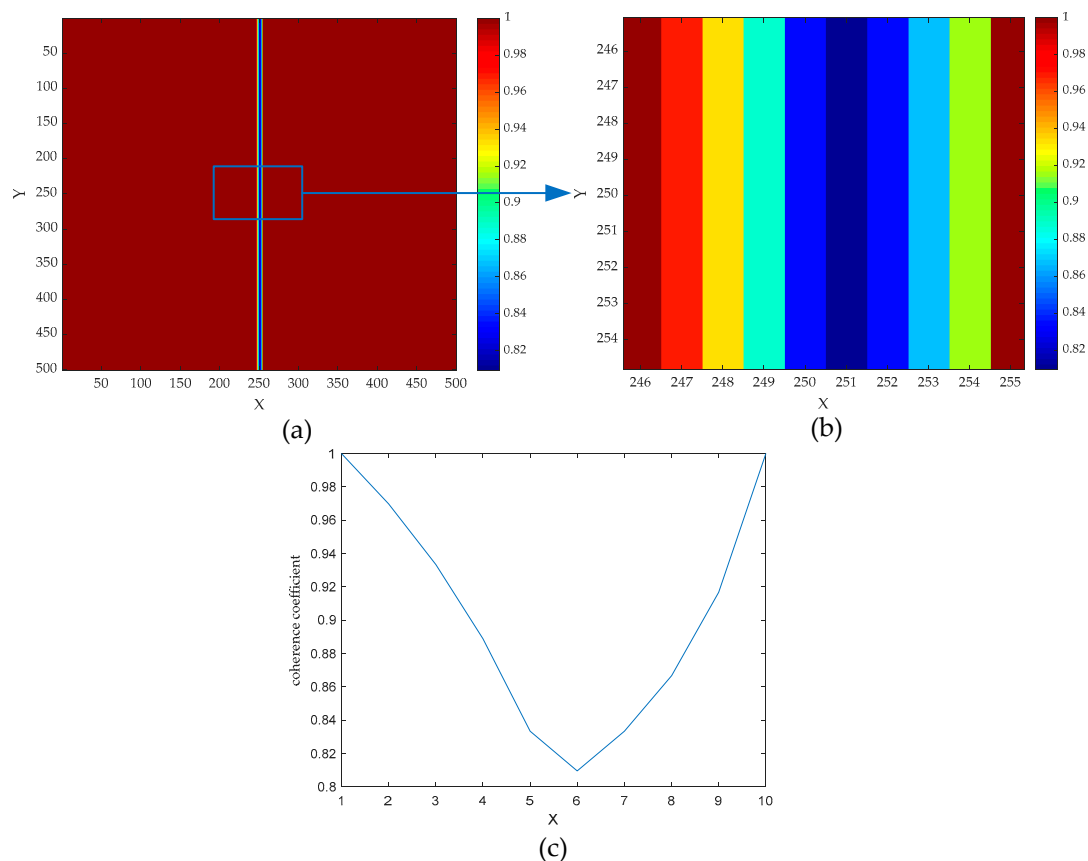
$$DC = \min\{r_i\} \quad i = 1, 2, 3, \dots, 16 \tag{16}$$

where *DC* is the directional coherent edge detection value.

Figure 4. Directional coherent edge detection model (DCEDM).

Edge detection was performed again with the above DCEDM. The results are shown in Figure 5. Figure 5a visualizes the obtained directional coherent edge detection coefficient. Figure 5b shows a partially enlarged display of Figure 5a. Figure 5c is a line chart of the directional coherent edge detection coefficient for any line of Figure 5b. Visually, the above problem encountered in the edge area of Figure 3b was effectively solved. As shown in Figure 5c, directional coherent edge detection coefficients were obtained at different positions of the edge region. The value was smallest at the center of the edge, which is in line with expectations. This is because a filter is expected to detect homogenous regions at a larger scale and edge regions at a smaller scale. Therefore, the above analysis proved the effectiveness of directional coherent edge detection.

Figure 5. Results of the directional coherent edge detection calculation: (**a**) directional coherent coefficient of the test image, (**b**) local display of (**a**), and (**c**) line graph of any line edge region of (**b**).

2.4. Method and Processes

The DCAD filter is an improved AD filter that is based on a PDE. The biggest difference between the proposed DCAD method and the already existing AD methods is the use of different edge detection operators: DCAD uses the directional coherence model to improve the edge detection operator. This obtains a more effective diffusion function to suppress speckle at each point of a SAR image. The novel edge detection operator *ETO* can be described as

$$ETO = DC = \min\left\{ r_i = \frac{\sum I_{Ai} \cdot I_{Bi}}{\sqrt{\sum I_{Ai}^2 \cdot \sum I_{Bi}^2}} \right\} \quad i = 1, 2, 3, \ldots, 16 \tag{17}$$

where the specific calculation models of r_i, $i = 1, 2, 3, \ldots, 16$ are represented in Figure 4 and *ETO* is 0–1. In a classical AD filter, the threshold of the edge detection operator needs to be set to obtain the diffusion function. However, a suitable threshold is difficult to determine, and an inaccurate estimate

often has adverse effects on speckle reduction. With the proposed method, the above problem can be ignored. The analysis presented in Section 2.4 showed that the directional coherent edge detection coefficient was higher in the homogeneous region of the test image and lower in the edge region. This is in line with the strategy of higher-scale suppression in homogeneous regions and lower-scale suppression in edge regions. Therefore, in the DCAD filter, *ETO* can directly play the role of the diffusion function *DF*:

$$DF = ETO. \tag{18}$$

The Jacobi iterative algorithm was used to solve the PDE of the AD filter; for details on this scheme, refer to Yu and Acton [25]. Figure 6 shows the solution process of the DCAD filter, which has the following steps:

1. Construct a new PDE with the directional coherent edge detection operator:

$$\begin{cases} \frac{\partial I}{\partial t} = div[DF \cdot \nabla I] \\ I(t=0) = I_0 \end{cases} . \tag{19}$$

2. Calculate *DF* with Equation (17) and Equation (18).
3. Calculate $div(DF \cdot \nabla I)$ with Equation (13).
4. Calculate the final filtering result with Equation (12).
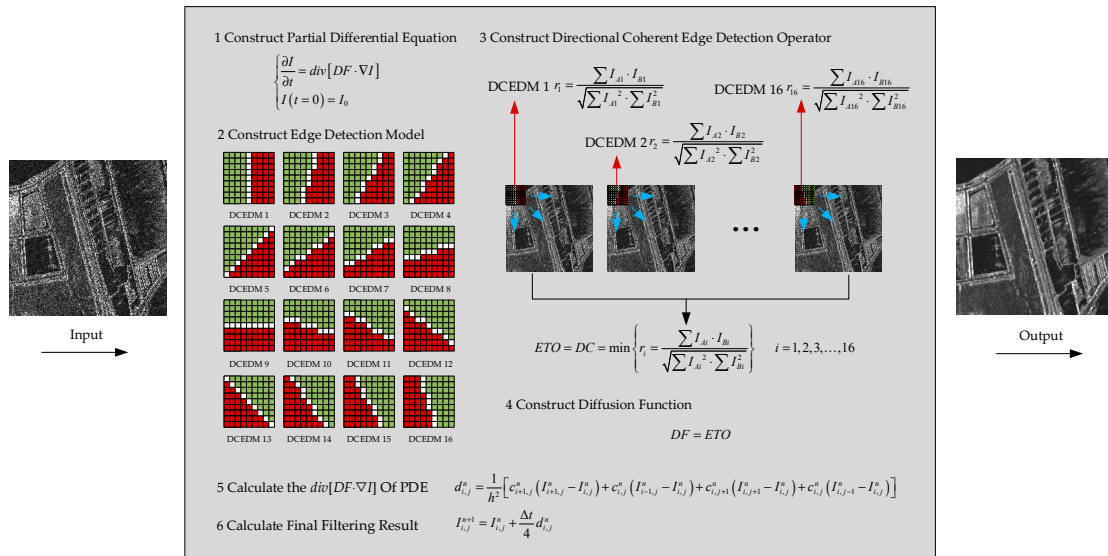
Figure 6. Flowchart of the proposed directional coherent anisotropic diffusion (DCAD) filtering method.

3. Results

3.1. Data Acquisition

The proposed algorithm was applied to a simulated image with multiplicative speckle noise to validate its effectiveness. A standard reference image with a size of 1000×1000 pixels was designed in MATLAB R2019a, as shown in Figure 7a. Subsequently, single look speckle was added according to Ferraioli et al.'s method [33], as shown in Figure 7b.

Next, three real SAR images from different sensors were selected to validate the proposed algorithm. The first real SAR image was from GF-3 in the C band, as shown in Figure 7c. The selected GF-3 SAR image was an SLC SAR image with HH polarization and a 3 m resolution in UFS mode. The second real SAR image was from TerraSAR-X in the X band, as shown in Figure 7d. The selected SLC TerraSAR-X SAR image was in SM mode and had the same polarization and resolution as the selected GF-3 image. The last real SAR image was from Rasarsat-2 in the C band, as shown in Figure 7e.

The selected SLC Radarsat-2 SAR image was in Rasarset-2 fine mode with HH polarization and an 8 m resolution. Both Figure 7 and the subsequent figures presenting the experimental results (see Figures 8–15) were cut to a size of 1000 × 1000 pixels to better display the results.
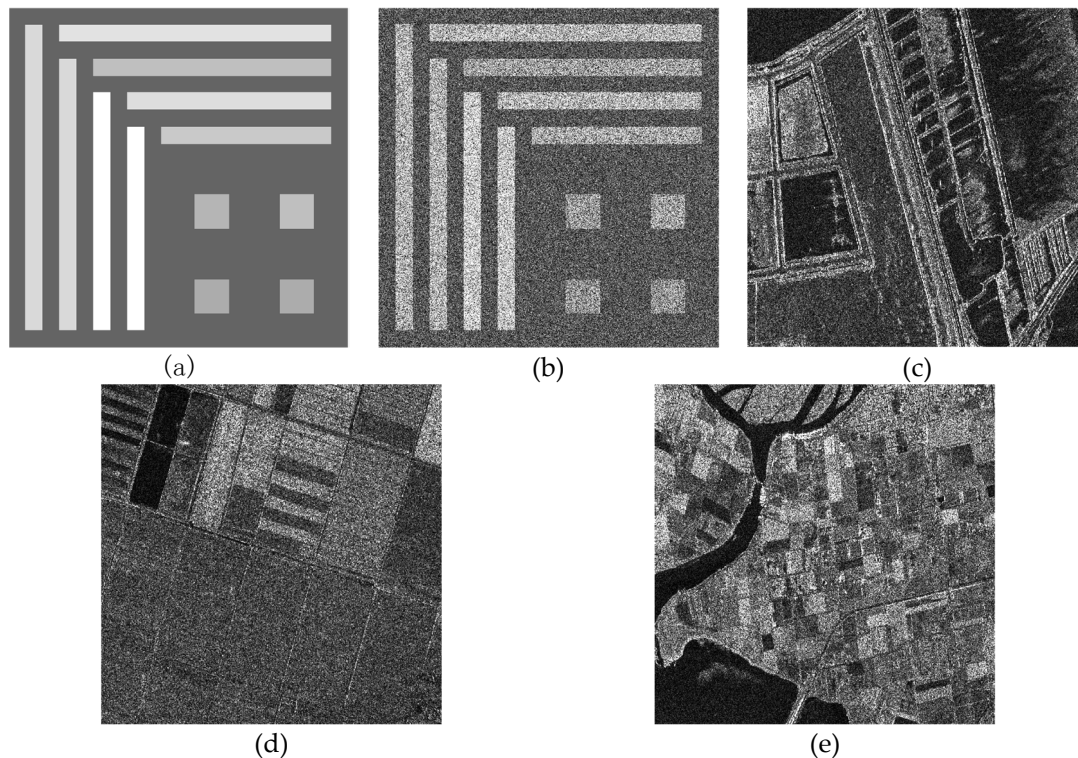
Figure 7. Experimental original images: (**a**) standard reference, (**b**) added multiplicative noise (single look), (**c**) GF-3 SAR, (**d**) TerraSAR-X SAR, and (**e**) Radarsat-2 SAR.

3.2. Method Selection

To evaluate the performance of the proposed algorithm, it was compared to other algorithms. To ensure the legibility of this article, it was only compared with the most popular approaches. Three kinds of filtering methods were selected to represent AD, SD, and TD filters. SRAD [25] is a classical AD filter that is often used for algorithm comparison. Improved AD filters are mostly based on the PDE of SRAD. Therefore, the SRAD filter was selected for comparison. The Lee filter [3] is a classical SD filter that was first proposed in the 1980s. Subsequently, a series of improved Lee filters [10–12] has been proposed to effectively suppress speckle. The improved Lee (I-Lee) [12] filter proposed in 2009 is often used for algorithm comparison. Therefore, the I-Lee filter was selected as the representative SD filter. Fast adaptive nonlocal SAR (FANS) [34] is a commonly selected TD filter for algorithm comparison. The FANS filter is an improved version of the well-known SARBM3D [35] algorithm, which has both excellent performance and low complexity. The codes of the above filters were acquired online. In subsequent experiments, the default parameters proposed by their respective authors were used. For the proposed DCAD method, the parameters were consistent with those of the SRAD filter: 300 iterations and a k value of 0.05.

3.3. Evaluation Methods

A good filtering effect needs not only visual evaluation, but also indicators for evaluation. SAR image denoising should smooth speckles and preserve edges and radiation. Therefore, the above three aspects need to be considered. The following four evaluation indices were selected:

1. The equivalent number of looks (ENL) indicates the speckle smoothing ability in homogeneous areas. For the actual evaluation, five homogeneous regions were randomly selected, and their average ENLs were used as the final ENL value. A higher ENL value indicates better smoothing.

2. The structural similarity (SSIM) [36] measures the edge preservation by the filter. The ideal value is 1, which corresponds to a high level of edge preservation.

3. The root mean square error (RMSE) was used to measure the radiation retention between the despeckled and noisy images. The ideal value of RMSE is 0, which corresponds to the expected radiation retention.

4. The M-index [37] can synthetically measure both speckle smoothing and edge preservation. The ideal value of the M-index is 0, which indicates that the filtering algorithm is performing well.

3.4. Experiment on Simulation Data

The simulated speckle image in Figure 7b was used first. The adopted methods and parameter settings are given in Section 3.2. The adopted evaluation methods are given in Section 3.3. The experimental results are shown in Figures 8 and 9. The index evaluation results are given in Table 1.
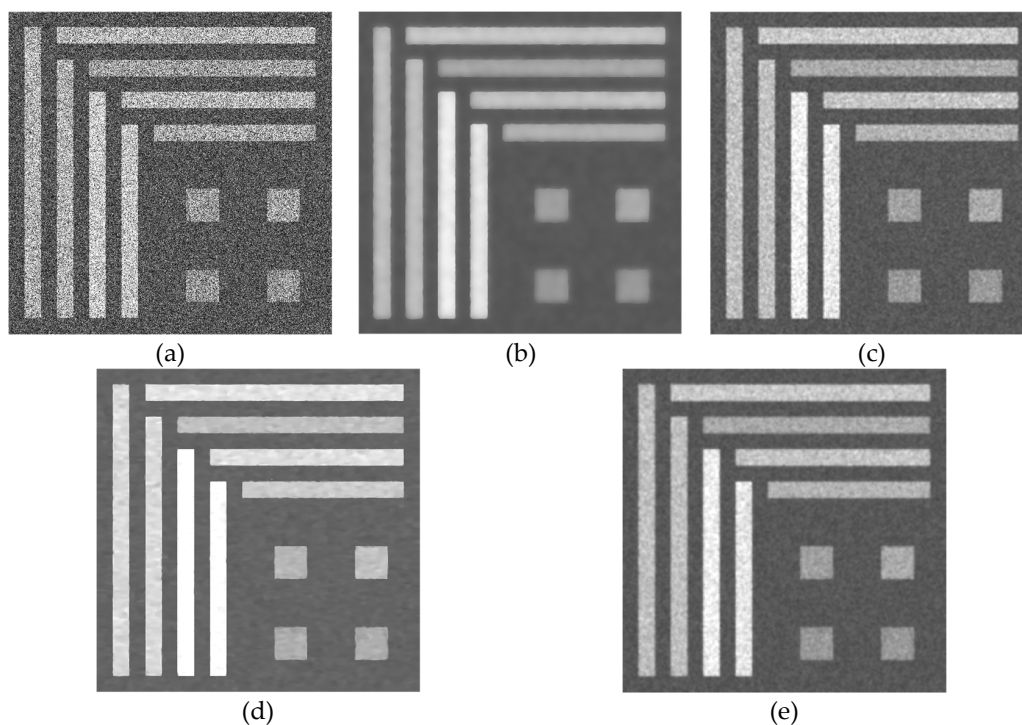
Figure 8. Filtered image with different denoising methods: (**a**) no filtering method, (**b**) SRAD filter, (**c**) I-Lee filter, (**d**) FANS filter, and (**e**) DCAD filter.
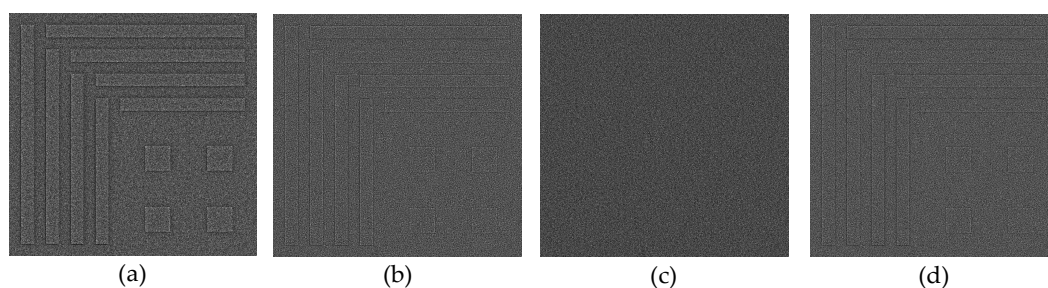
Figure 9. Ratio image between the original and filtered images with different filtering methods: (**a**) SRAD filter, (**b**) I-Lee filter, (**c**) Fast adaptive nonlocal SAR (FANS) filter, and (**d**) DCAD filter.

Table 1. Index evaluation of the filtering performance for the simulated image. ENL: equivalent number of looks; SSIM: structural similarity; RMSE: root mean square error.

	IDEAL	None	SRAD	I-Lee	FANS	DCAD
ENL	Large	4	2487	269	1358	310
SSIM	1	—	0.53	0.56	0.58	0.58
RMSE	0	—	57.15	56.74	61.16	56.06
M-Index	0	—	78.44	63.05	42.76	46.32

Figure 8 shows that the speckle was effectively suppressed by all four filters. However, differences still existed between filters. Although the SRAD filter effectively suppressed speckle, the filtered image was too smooth (Figure 8b). The overly smooth image resulted in the loss of many details, which was not the expected result. Visually, the FANS, DCAD, and I-Lee filters performed better than the SRAD filter. The DCAD filter provided slightly better noise smoothing than the I-Lee filter. The FANS filter performed best in locally homogeneous regions, followed by the DCAD filter. For the simulation data, the FANS filter achieved good filtering and benefited from the simulated data being composed of several pixel blocks, which was very helpful for classification. In real SAR images, there would be many more amplitudes.

The ratio images between the original and denoised SAR images partially reflect the edge preservation performance. With a perfect filter, the ratio image should contain speckle and no other object details. Figure 9 shows the ratio images obtained from the denoising experiment with simulated data. The ratio image with the SRAD filter contains many obvious details, which again indicates loss from oversmoothing. The ratio images obtained by the I-Lee and DCAD filters showed slight residual detail, and the FANS filter left almost invisible details.

For a more comprehensive evaluation of the filtering effect, the above indices were evaluated, and the corresponding results are presented in Table 1. The SRAD filter achieved the highest ENL value (2048) among the four methods. However, it performed the worst for SSIM (0.53), RMSE (57.15), and M-index (78.44). The I-Lee filter obtained the lowest ENL value (269). The ENL of the original image was just 4, which means that the original ENL was tremendously improved after the I-Lee filter. Visual inspection showed that speckle was effectively suppressed. The DCAD filter had a higher ENL value (310) than the I-Lee filter that was more than 70 times higher than the original image. This indicates that the DCAD filter provided good smoothing. The FANS and DCAD filters had the same performance for SSIM and performed better than the SRAD and I-Lee filters. The good performance in SSIM indicates good edge preservation and is consistent with the ratio image results. The DCAD filter had the best RMSE, while the FANS filter performed the worst. This indicates that the DCAD filter had the best radiation retention among the four methods. The FANS filter had the best M-index value followed by the DCAD filter. This indicates that the FANS and DCAD filters provided excellent filtering. Overall, the performance of the DCAD filter effectively verified its feasibility and superiority for simulated data.

3.5. Experiment on Actual SAR Data

An experiment was next conducted on real SLC SAR images (see Figure 7c–e). The adopted methods and parameter settings are given in Section 3.2. The adopted evaluation methods are given in Section 3.3. The results for the GF-3 SAR image, TerraSAR-X SAR image, and Radarsat-2 SAR image are given below.

3.5.1. Experiment on the GF-3 SAR Image

Figure 10 shows the filtering results for the GF-3 SAR image. Similar to the simulation experiment, speckle was effectively suppressed, but the differences between the methods became more prominent. The SRAD filter lost more edge information and had more obvious oversmoothing, as shown in Figure 10b. Figure 10c shows that the I-Lee filter effectively suppressed the speckle. However, there

were a few independent strong points that did not match the neighborhood radiation information. Figure 10d shows that the FANS filter effectively suppressed the speckle. However, some cluttered and tiny textures were erroneously generated in the denoised image. Figure 10e shows that the DCAD filter provided an excellent performance. Overall, it provided a superior visual result compared to the SRAD, I-Lee, and FANS filters. Figure 11 shows the ratio images, which are similar to the simulation results. The SRAD filter performed the worst and left some obvious details, while the other three methods left only a small amount of detail. Table 2 presents the results of the evaluation indices. For ENL, all four methods performed well, and the lowest ENL (91 by the I-Lee filter) was at least 30 times the original ENL value (3). The SRAD filter obtained the highest ENL (999), followed by the DCAD filter (195). For SSIM, the DCAD, FANS, and I-Lee filters performed better than the SRAD filter, and the DCAD filter performed the best. For RMSE, the FANS filter performed the best, followed by the DCAD filter. For the M-index, the DCAD filter performed the best and the FANS filter performed the worst. These results verify the feasibility and superiority of the DCAD filter for the GF-3 SAR image.
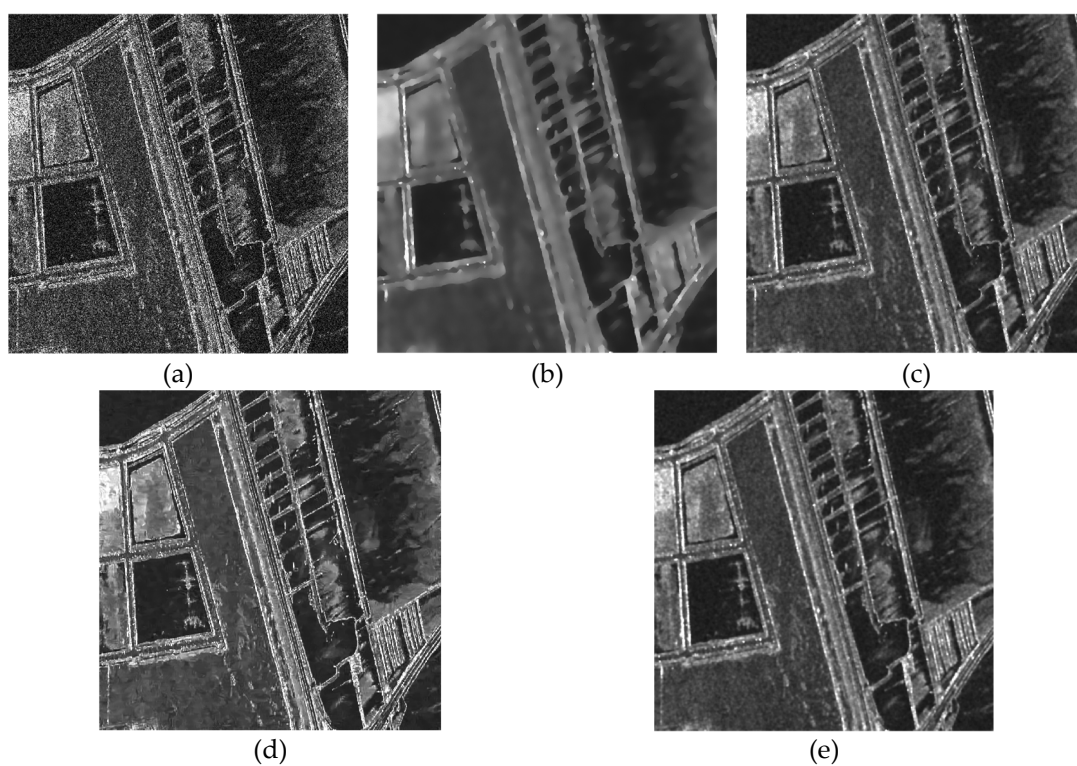
Figure 10. Filtered image with different denoising methods: (**a**) no filtering method, (**b**) SRAD filter, (**c**) I-Lee filter, (**d**) FANS filter, and (**e**) DCAD filter.
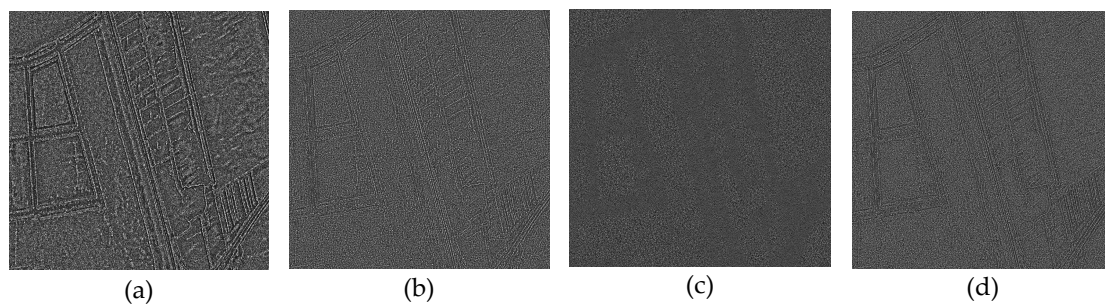
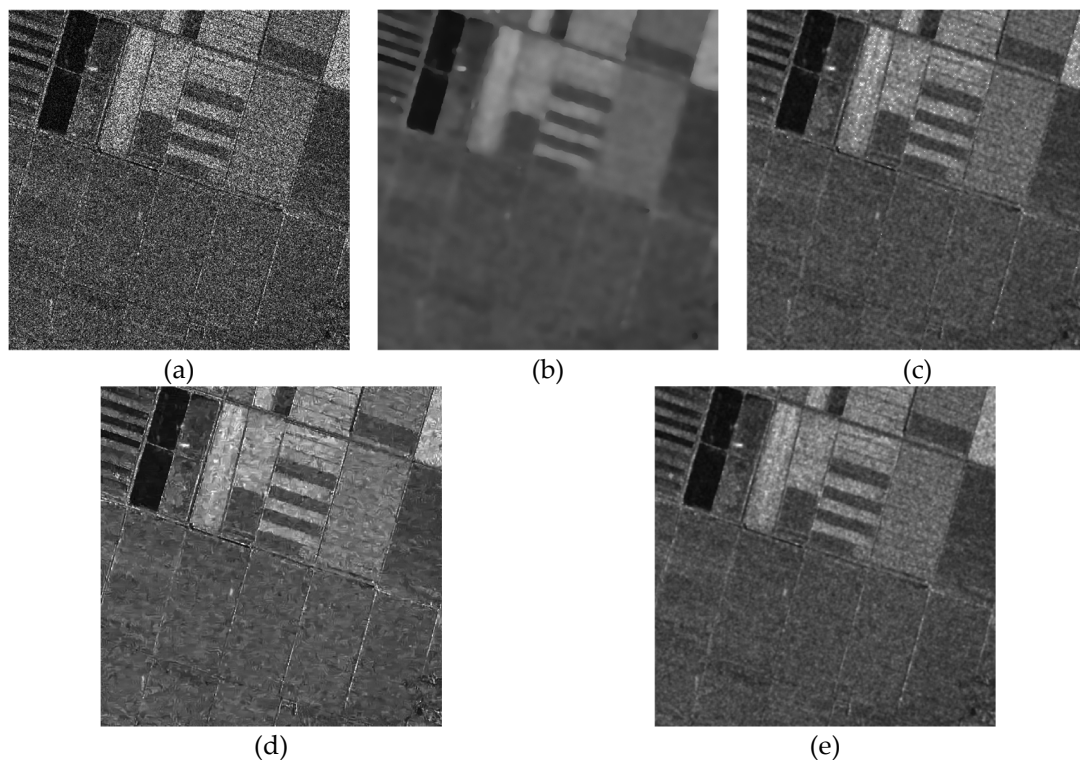**Figure 11.** Ratio image between the original and filtered images with different filtering methods: (**a**) SRAD filter, (**b**) I-Lee filter, (**c**) FANS filter, and (**d**) DCAD filter.

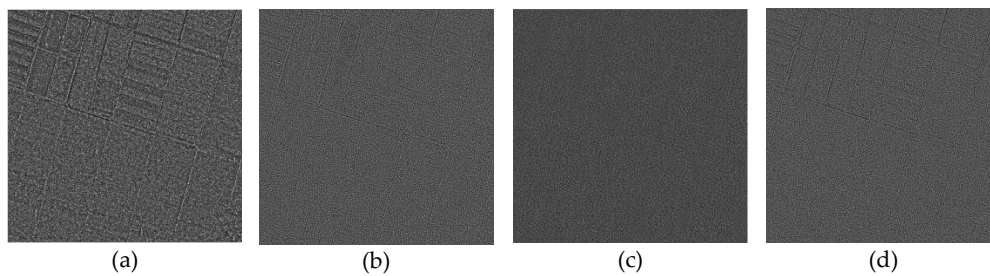**Table 2.** Index evaluation for the filtering performance of the GF-3 SAR image.

	IDEAL	None	SRAD	I-Lee	FANS	DCAD
ENL	Large	3	999	91	158	195
SSIM	1	—	0.55	0.63	0.65	0.69
RMSE	0	—	49.2	43.2	36.35	37.39
M-Index	0	—	23.38	16.79	29.42	15.99

3.5.2. Experiment on the TerraSAR-X SAR Image

Figure 12 shows that the abundant speckle in the original image (see Figure 12a) was effectively suppressed by all four filters. For the TerraSAR-X SAR image, the SRAD filter still caused oversmoothing (Figure 12b). Incongruous strong points also were present with the I-Lee filter (Figure 12c). The unwanted, cluttered, and tiny textures were more obvious in the denoised image with the FANS filter (Figure 12d). Similar to the GF-3 SAR image, the DCAD filter performed best visually (Figure 12e). The ratio images in Figure 13 show that the SRAD filter left obvious details, while the other methods left a small amount of detail. For the evaluation indices, the DCAD filter had the best M-index, and the FANS filter had the worst. In Table 3, the FANS filter had the best SSIM and RMSE values, followed by the DCAD filter. For ENL, the I-Lee, FANS, and DCAD filters had relatively close results; the lowest ENL (89) was at least 20 times as much as the original ENL (4). Therefore, the feasibility and superiority of the DCAD filter were verified for the TerraSAR-X SAR image.

Figure 12. Filtered image with different denoising methods: (**a**) no filtering method, (**b**) SRAD filter, (**c**) I-Lee filter, (**d**) FANS filter, and (**e**) DCAD filter.
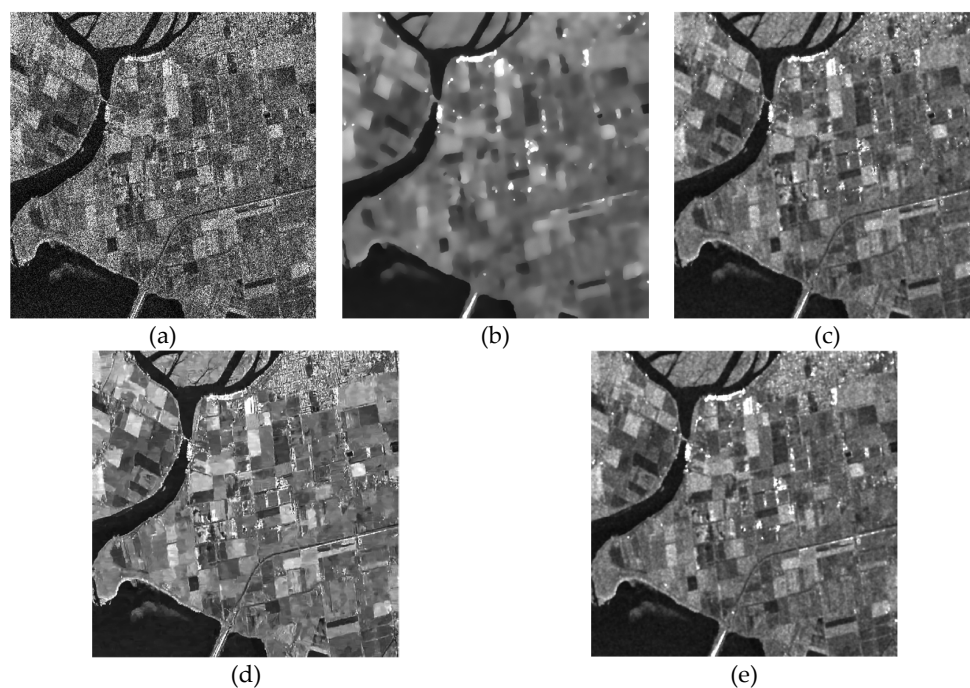
Figure 13. Ratio image between the original and filtered images with different filtering methods: (**a**) SRAD filter, (**b**) I-Lee filter, (**c**) FANS filter, and (**d**) DCAD filter.

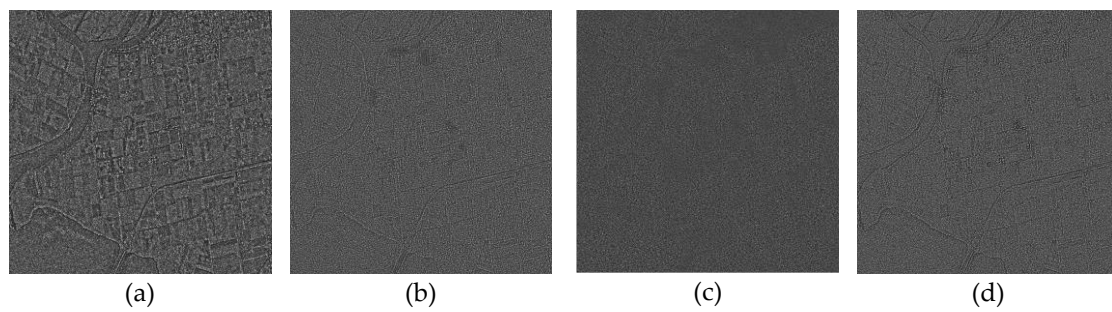**Table 3.** Index evaluation for the filtering performance of the TerraSAR-X SAR image.

	IDEAL	None	SRAD	I-Lee	FANS	DCAD
ENL	Large	4	1252	89	98	93
SSIM	1	—	0.44	0.55	0.59	0.55
RMSE	0	—	45.01	42.51	39.61	41.73
M-Index	0	—	10.61	10.45	11.40	6.73

3.5.3. Experiment on the Radarsat-2 SAR Image

Similar to the previous experimental results, the above four filters achieved good speckle smoothing, as shown in Figure 14. The SRAD and I-Lee filters still resulted in oversmoothing and inconsistent strong points, respectively. Overall, the FANS and DCAD filters performed relatively well visually. The ratio images shown in Figure 15 indicate that the FANS filter left behind a few details, while the I-Lee and DCAD filters left a very small amount of detail. The most detail was left behind by the SRAD filter. From Table 4, the DCAD filter performed the best in terms of RMSE and M-index. For SSIM, the FANS, I-Lee, and DCAD filters performed comparably. For ENL, all four methods showed great improvement compared to the original ENL (3), and the lowest ENL (112) was an increase of more than 35 times. Therefore, the results effectively verified the feasibility and superiority of the DCAD filter for the Radarsat-2 SAR image.

Figure 14. Filtered image with different denoising methods: (**a**) no filtering method, (**b**) SRAD filter, (**c**) I-Lee filter, (**d**) FANS filter, and (**e**) DCAD filter.

Figure 15. Ratio image between the original and filtered images with different filtering methods: (**a**) SRAD filter, (**b**) I-Lee filter, (**c**) FANS filter, and (**d**) DCAD filter.

**Table 4.** Index evaluation for the filtering performance of the Radarsat-2 SAR image.

	IDEAL	None	SRAD	I-Lee	FANS	DCAD
ENL	Large	3	747	112	156	119
SSIM	1	—	0.47	0.66	0.68	0.67
RMSE	0	—	54.35	50.66	47.58	46.88
M-Index	0	—	15.27	7.63	13.10	9.82

4. Discussion

For AD filters, different parameter settings affect the results. For the proposed DCAD, the influence of parameters such as the number of iterations, time step, and spatial step were analyzed. In general, the spatial step size was often set to 1. Therefore, the rest of this section mainly discusses the influence of the number of iterations and time step on the results of the DCAD filter.

4.1. Influence of Number of Iterations on the DCAD Filter

The GF-3 SAR image (see Figure 7c) was selected as the experimental image. The adopted evaluation methods are given in Section 3.3. The time step was set to 0.05, the number of iterations was set from 10 to 400 with intervals of 10. The results of the index evaluation are shown in Figure 16.
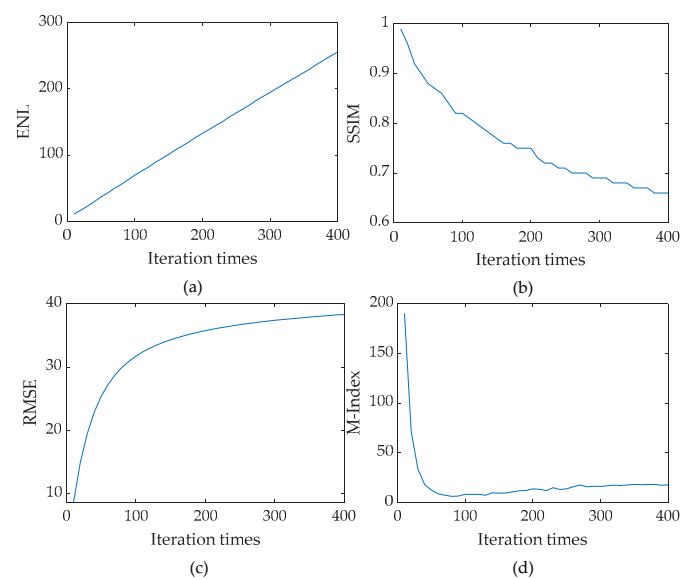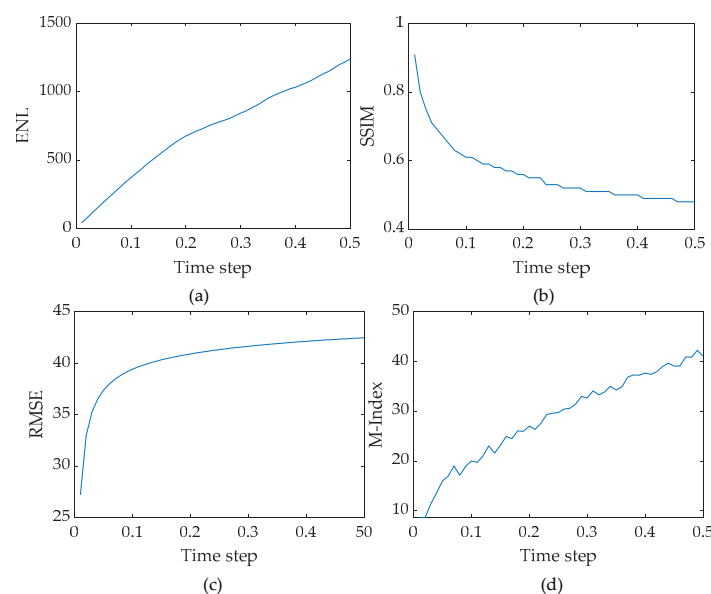

Figure 16. Influence of the number of iterations on the DCAD filter: index evaluations with (**a**) ENL, (**b**) SSIM, (**c**) RMSE, and (**d**) M-Index.

Figure 16a shows that ENL increased continuously and almost linearly with the number of iterations. This phenomenon indicates that the number of iterations significantly affects speckle

smoothing. Figure 16b,c show that both the edge and radiation preservation performances decreased as the number of iterations increased. Figure 16d shows that the M-index initially decreased rapidly and then increased slowly as the number of iterations increased. This means that both small and large numbers of iterations are not the best choice. These results indicate that increasing the number of iterations affects different aspects of filtering that need to be balanced to obtain better results. To get better speckle smoothing, a relatively large number of iterations should be used. To get better edge and radiation retention, a relatively small number of iterations is preferred. According to the M-index results, the number of iterations should be between 150 and 330 at a time step of 0.05.

4.2. Influence of the Time Step on the DCAD Filter

The GF-3 SAR image (see Figure 7c) was selected as the experimental image. The adopted evaluation methods are given in Section 3.3. The number of iterations was set to 300 and the time step was set from 0.01 to 0.5 in intervals of 0.01. The index evaluation results are shown in Figure 17.

Figure 17. Influence of the time step on the DCAD filter: index evaluations with (**a**) ENL, (**b**) SSIM, (**c**) RMSE, and (**d**) M-Index.

The ENL, SSIM, and RMSE results showed that increasing the time step had a similar effect to that of increasing the number of iterations. As the time step increased, ENL and RMSE increased and SSIM decreased. This indicates increased smoothing but worsening edge and radiation retention. These results indicate that the time step should be large to improve the speckle smoothing, while the time step should be small to improve the edge and radiation retention. The M-index increased with the time step, which indicates that increasing the time step was disadvantageous. The experimental results suggest that the time step should not exceed 0.2 when the number of iterations is set to 300.

5. Conclusions

This paper proposes the novel DCAD filter, which uses a directional coherent coefficient to improve the edge detection operator and effectively achieve better edge detection. The DCAD filter directly uses the detected directional coherent edge as the diffusion coefficient, which simplifies the calculation of the diffusion function of the traditional AD filter and avoids the adverse effects of inaccurate estimation of the diffusion function threshold. Speckle suppression experiments were carried out using simulated data and real SAR images, and the results demonstrated that the proposed DCAD filter can effectively suppress speckle and preserve edges and radiation information. The influences of the number of iterations and size of the time step on the DCAD filter were evaluated, and the experimental

results showed that the number of iterations and the time step should be relatively large to get better speckle smoothing and relatively small to get better edge and radiation retention. The effectiveness and excellent performance of the DCAD filter support its potential use in a number of SAR imaging applications. The main limitation of the proposed method is related to the computational complexity. Since it uses 16 different coherent edge detection models, the computational complexity of the DCAD method is increased accordingly. However, the use of the parallelization of the code could help in improving this aspect. In addition, only classical filters were used for comparisons in this paper. Our future work will therefore focus on comparisons with the newest filters.

Conflicts of Interest: The authors declare no conflict of interest.

References

1. Oliver, C.; Quegan, S. *Understanding Synthetic Aperture Radar Images*; Artech House: Boston, MA, USA, 1998.
2. Argenti, F.; Lapini, A.; Bianchi, T.; Alparone, L. A Tutorial on Speckle Reduction in Synthetic Aperture Radar Images. *IEEE Geosci. Remote Sens. Mag.* **2013**, *1*, 6–35. [CrossRef]
3. Tounsi, Y.; Kumar, M.; Nassim, A.; Mendoza-Santoyo, F.; Matoba, O. Speckle denosing by variant nonlocal means methods. *Appl. Optics* **2019**, *58*, 7110–7210. [CrossRef] [PubMed]
4. Tounsi, Y.; Kumar, M.; Nassim, A.; Mendoza-Santoyo, F. Speckle noise reduction in digital speckle pattern interferometric fringes by nonlocal means and its related adaptive kernel-based methods. *Appl. Opt.* **2018**, *57*, 7681–7690. [CrossRef] [PubMed]
5. Zada, S.; Tounsi, Y.; Kumar, M.; Mendoza-Santoyo, F.; Nassim, A. Contribution study of monogenic wavelets transform to reduce speckle noise in digital speckle pattern interferometry. *Opt. Eng.* **2019**, *58*, 034109. [CrossRef]
6. Buades, A.; Coll, B.; Morel, J.-M. A Non-Local Algorithm for Image Denoising. In Proceedings of the 2005 IEEE Computer Society Conference on Computer Vision and Pattern Recognition (CVPR 05), San Diego, CA, USA, 20–25 June 2005; Volume 2, pp. 60–65.
7. Ery, A.C.; Salmon, J.; Willett, R. Oracle inequalities and minimax rates for nonlocal means and related adaptive kernel-based methods. *SIAM J. Imaging Sci.* **2013**, *5*, 944–992.
8. Coupé, P.; Hellier, P.; Kervrann, C.; Barillot, C. Nonlocal means-based speckle filtering for ultrasound images. *IEEE Trans. Image Process.* **2009**, *18*, 2221–2229. [CrossRef]
9. Lee, J.-S. Digital Image Enhancement and Noise Filtering by Use of Local Statistics. *IEEE Trans. Pattern Anal. Mach. Intell.* **1980**, 165–168. [CrossRef]
10. Lee, J.-S. Refined filtering of image noise using local statistics. *Comput. Graph. Image Process.* **1981**, *15*, 380–389. [CrossRef]
11. Lee, J.-S. Digital image smoothing and the sigma filter. *Comput. Vision, Graph. Image Process.* **1983**, *24*, 255–269. [CrossRef]
12. Lee, J.S.; Wen, J.H.; Ainsworth, T.L.; Chen, K.S.; Chen, A.J. Improved sigma filter for speckle filtering of SAR imagery. *IEEE Trans. Geosci. Remote Sens.* **2009**, *47*, 202–213.
13. Frost, V.S.; Stiles, J.A.; Shanmugan, K.S.; Holtzman, J.C. A Model for Radar Images and Its Application to Adaptive Digital Filtering of Multiplicative Noise. *IEEE Trans. Pattern Anal. Mach. Intell.* **1982**, 157–166. [CrossRef] [PubMed]

14. Touzi, R. A review of speckle filtering in the context of estimation theory. *IEEE Trans. Geosci. Remote Sens.* **2002**, *40*, 2392–2404. [CrossRef]

15. Kuan, D.T.; Sawchuk, A.A.; Strand, T.C.; Chavel, P. Adaptive Noise Smoothing Filter for Images with Signal-Dependent Noise. *IEEE Trans. Pattern Anal. Mach. Intell.* **1985**, 165–177. [CrossRef] [PubMed]

16. Lopes, A.; Touzi, R.; Nezry, E. Adaptive speckle filters and scene heterogeneity. *IEEE Trans. Geosci. Remote Sens.* **1990**, *28*, 992–1000. [CrossRef]

17. Xie, H.; Pierce, L.; Ulaby, F. SAR speckle reduction using wavelet denoising and Markov random field modeling. *IEEE Trans. Geosci. Remote Sens.* **2002**, *40*, 2196–2212. [CrossRef]

18. Achim, A.; Tsakalides, P.; Bezerianos, A. SAR image denoising via Bayesian wavelet shrinkage based on heavy-tailed modeling. *IEEE Trans. Geosci. Remote Sens.* **2003**, *41*, 1773–1784. [CrossRef]

19. Ranjani, J.J.; Thiruvengadam, S.J. Dual-Tree Complex Wavelet Transform Based SAR Despeckling Using Interscale Dependence. *IEEE Trans. Geosci. Remote Sens.* **2010**, *48*, 2723–2731. [CrossRef]

20. Liu, S.; Shi, M.; Hu, S.; Xiao, Y. Synthetic aperture radar image de-noising based on Shearlet transform using the context-based model. *Phys. Commun.* **2014**, *13*, 221–229. [CrossRef]

21. Guo, F.; Zhang, G.; Zhang, Q.; Zhao, R.; Deng, M.; Xu, K. Speckle Suppression by Weighted Euclidean Distance Anisotropic Diffusion. *Remote Sens.* **2018**, *10*, 722. [CrossRef]

22. Zhu, L. *Study on Speckle Reduction Methods for Synthetic Aperture Radar Images*; Xidian University: Xi'an, China, 2013.

23. Li, J.C. *The Research on Speckle Reduction for Synthetic Aperture Radar Images*; National University of Defense Technology: Changsha, China, 2014.

24. Perona, P.; Malik, J. Scale-space and edge detection using anisotropic diffusion. *IEEE Trans. Pattern Anal. Mach. Intell.* **1990**, *12*, 629–639. [CrossRef]

25. Yu, Y.; Acton, S. Speckle reducing anisotropic diffusion. *IEEE Trans. Image Process.* **2002**, *11*, 1260–1270. [PubMed]

26. Aja-Fernández, S.; Alberola-López, C. On the estimation of the coefficient of variation for anisotropic diffusion speckle filtering. *IEEE Trans. Image Process.* **2006**, *15*, 2694–2701. [CrossRef] [PubMed]

27. Liu, G.; Zeng, X.; Tian, F.; Li, Z.; Chaibou, K. Speckle reduction by adaptive window anisotropic diffusion. *Signal Process.* **2009**, *89*, 2233–2243. [CrossRef]

28. Mishra, D.; Chaudhury, S.; Sarkar, M.; Soin, A.S.; Sharma, V. Edge Probability and Pixel Relativity-Based Speckle Reducing Anisotropic Diffusion. *IEEE Trans. Image Process.* **2018**, *27*, 649–664. [CrossRef]

29. Li, J.C.; Ma, Z.H.; Peng, Y.X.; Huang, H. Speckle reduction by image entropy anisotropic diffusion. *Acta Phys. Sin.* **2013**, *62*, 099501.

30. Frery, A.C.; Yanasse, C.d.C.F.; Santa'Anna, S.J.S. *Statistical Characterization of SAR Data: The Multiplicative Model and Extensions*; Simposio Latinoamericano de Especialistas en Percepcion Remota: Puerto Vallarta, Mexico, 1995.

31. Touzi, R.; Lopes, A.; Bruniquel, J. Coherence estimation of SAR imagery. *IEEE Trans. Geosci. Remote Sens.* **1999**, *37*, 135–149. [CrossRef]

32. Zhang, H.; Wang, C.; Wu, T.; Tang, Y.X. *Research on DInSAR Method Based on Coherent Target*; Science Press: Beijing, China, 2009.

33. Ferraioli, G.; Pascazio, V.; Schirinzi, G. Ratio-Based Nonlocal Anisotropic Despeckling Approach for SAR Images. *IEEE Trans. Geosci. Remote Sens.* **2019**, *57*, 7785–7798. [CrossRef]

34. Cozzolino, D.; Parrilli, S.; Scarpa, G.; Poggi, G.; Verdoliva, L. Fast adaptive nonlocal SAR despeckling. *IEEE Geosci. Remote Sens. Lett.* **2014**, *11*, 524–528. [CrossRef]

35. Dabov, K.; Foi, A.; Katkovnik, V.; Egiazarian, K. Image denoising by sparse 3-D transform-domain collaborative filtering. *IEEE Trans. Image Process.* **2007**, *16*, 2080–2095. [CrossRef]

36. Wang, Z.; Bovik, A.; Sheikh, H.; Simoncelli, E. Image Quality Assessment: From Error Visibility to Structural Similarity. *IEEE Trans. Image Process.* **2004**, *13*, 600–612. [CrossRef]

37. Gomez, L.; Ospina, R.; Frery, A.C. Unassisted Quantitative Evaluation of Despeckling Filters. *Remote Sens.* **2017**, *9*, 389. [CrossRef]